Huchon, P., Taylor, B., and Klaus, A. (Eds.)
Proceedings of the Ocean Drilling Program, Scientific Results Volume 180

17. Data Report: Trace Element and Isotopic Composition of Interstitial Water and Sediments from the Woodlark Rise, ODP Leg 180[1]

Eric Heinen De Carlo,[2] Klas K. Lackschewitz,[3]
and Rebecca Carmody[4]

ABSTRACT

Oxygen and strontium isotopes and Rb and Ba were determined in interstitial water (IW) collected from Sites 1109, 1115, and 1118 drilled on the Woodlark Rise during Ocean Drilling Program Leg 180. The trace element and mineralogical composition of the clay fraction of sediments isolated from the squeeze cakes corresponding to IW samples from Site 1109 was also determined.

INTRODUCTION

During Ocean Drilling Program (ODP) Leg 180, a series of holes was drilled in the Woodlark Basin to characterize the composition and in situ properties (stress, permeability, temperature, pressure, physical properties, and fluid pressure) of an active low-angle normal fault zone (Taylor, Huchon, Klaus, et al., 1999). The western Woodlark Basin is characterized by a lateral variation from active continental rifting to seafloor spreading within a small region, and in the northern margin of the basin, the Woodlark Rise represents a downflexed prerift sedimentary basin and basement sequence that is unconformably onlapped by synrift sediments. A north-south transect of three deep holes (Sites 1109, 1115, and 1118), representing a spatial proxy for the temporal

[1] De Carlo, E.H., Lackschewitz, K.K., and Carmody, R., 2001. Data report: Trace element and isotopic composition of interstitial water and sediments from the Woodlark Rise, ODP Leg 180. *In* Huchon, P., Taylor, B., and Klaus, A. (Eds.), *Proc. ODP, Sci. Results,* 180, 1–20 [Online]. Available from World Wide Web: <http://www-odp.tamu.edu/publications/180_SR/VOLUME/CHAPTERS/160.PDF>. [Cited YYYY-MM-DD]
[2] Department of Oceanography, SOEST, University of Hawaii at Manoa, Honolulu HI 96822, USA. edecarlo@soest.hawaii.edu
[3] Fachgebiet Petrologie der Ozeankruste, Fachbereich 5, Geowissenschaften Postfach 330 440, 28334 Bremen, Federal Republic of Germany.
[4] SOEST, University of Hawaii at Manoa, Honolulu HI 96822, USA.

Initial receipt: 14 December 2000
Acceptance: 7 July 2001
Web publication: 2 November 2001
Ms 180SR-160

variability of tectonic activity in the area, was drilled on the Woodlark Rise.

In this paper we present results of isotopic ($^{87}Sr/^{86}Sr$ and $\delta^{18}O$) and trace element (Rb and Ba) analyses in interstitial water (IW) from the three sites and the trace element composition and mineralogy of corresponding sediments at Site 1109. A subset of squeeze cakes remaining after IW was recovered from whole-round cores collected at Site 1109 was selected on the basis of volcanic matter content. The clays were analyzed for their trace element content to evaluate how the presence and alteration of volcanic minerals impact the chemical composition of the IW.

Volcanic matter in sediments of the Woodlark Rise is present as discrete ash layers and dispersed volcaniclastic sand, as well as large-body intrusions or basement igneous rocks deep in the holes (Taylor, Huchon, Klaus, et al., 1999). Sediments cored at Site 1109 record progressive subsidence from subaerial to lagoonal then shallow- to deep-water marine settings between the latest Miocene (~8 Ma) and the late Pleistocene. The hemipelagic Pliocene sediments (i.e., the upper ~550 meters below seafloor [mbsf]) include an abundance of volcanic ash layers and dispersed volcanic material, much of which is quite fresh and unaltered (Taylor, Huchon, Klaus, et al., 1999). Interpretations of the data reported here will be presented elsewhere (De Carlo et al., unpubl. data).

METHODS

High-resolution sampling at Sites 1109 and 1115 successfully recovered IW from whole rounds taken from nearly every recovered sedimentary core in each hole. At Site 1118 where the first 200 mbsf was drilled without coring, a lower-resolution sampling program was undertaken with whole rounds collected every second or third core beginning near 250 mbsf. The suite of 26 IW samples obtained at Site 1118 complements the more than 130 IW samples collected from Sites 1109 and 1115.

Methods for recovery of IW and details of the sample handling and shipboard analyses are described in Taylor, Huchon, Klaus, et al. (1999) and are only briefly described here. IW was recovered by mechanical squeezing of 5- to 15-cm whole-round cores in a titanium squeezer, modified after the standard ODP stainless steel squeezer of Manheim and Sayles (1974), to provide contamination-free IW samples. Samples were initially collected from the squeezer through 0.45-µm Gelman polysulfone disposable filters into scrupulously cleaned 50-mL plastic syringes. IW to be used for trace element analysis was filtered through acid-washed 0.2-µm Gelman polysulfone disposable filters, transferred to acid-washed high-density polyethylene bottles, acidified with 50 µL of ultra-high purity HNO_3, and stored chilled until analysis. Samples for isotopic analyses were transferred from the syringe to glass vials without additional filtering and immediately sealed.

Dissolved Ba was determined by inductively coupled plasma–optical emission spectroscopy (ICP-OES) using a Leeman Labs model PS1 echelle grating spectrometer (e.g., De Carlo, 1992) or by mass spectrometry (ICP-MS) using a VG Plasma Quad II-S instrument. The ICP-OES was calibrated using a series of standards prepared by addition of single-element standards (Ba^{2+}) to a NaCl matrix, as described by De Carlo and Kramer (2000). The ICP-MS was calibrated using a series of aqueous

standards diluted from a NIST-traceable stock multielement standard. Instrument drift was monitored at masses 115, 147, and 209 using In, Sm, and Bi as internal standards.

Dissolved Rb^+ was determined by atomic emission spectrometry (AES) using the method of standard addition on a Perkin Elmer Model 603 double-beam spectrometer. The atomic emission of Rb was measured at 780 nm using a 0.2-nm slit width. Because IW can show wide variations in matrix composition (e.g., salt concentrations), a background correction technique developed in our laboratory for analysis of geothermal and hydrothermal fluids was used (Fraley and De Carlo, unpubl. data). This method compensates for the large background absorption signals often encountered in high-salinity fluids (e.g., De Carlo and Kramer, 2000). A subgroup of IW samples was analyzed for Rb by AES and by ICP-MS to evaluate the comparability of results obtained by the two methods. The methods generally yielded comparable results, although the ICP-MS data seem biased toward lower values than the results obtained by AES.

The oxygen isotopic composition of the pore water samples was determined in the Isotope Biogeochemical Laboratory at the University of Hawaii using a microscale adaptation of Epstein and Mayeda's (1953) CO_2–H_2O equilibration method, described by Tüchsen et al. (1987). Aliquots of water (120 mg, measured gravimetrically) were equilibrated with 22 µmol of CO_2 (measured using a calibrated Baratron gauge) at 22°C for at least 48 hr. The oxygen isotopic composition of purified CO_2 was measured using a Finnigan MAT 252 isotope-ratio mass spectrometer. Oxygen isotopic data are expressed in per mil (‰) deviation from the VSMOW (Vienna standard mean ocean water) standard:

$$\delta^{18}O = \{[(^{18}O/^{16}O)_{smpl}/(^{18}O/^{16}O)_{VSMOW}]-1\} \times 100.$$

The $\delta^{18}O$ values are normalized such that the $\delta^{18}O$ value of standard light Antarctic precipitation is –55.5‰. The 2-σ precision for replicate $\delta^{18}O$ analyses of samples and the VSMOW standard is ±0.2‰.

The isotopic composition of dissolved strontium in the pore water samples was determined at the University of Hawaii Radiogenic Isotope Laboratory. The method used for analyzing strontium isotopic samples in this laboratory was described by Mahoney et al. (1991). The following modifications were applied in the current study: aliquots of pore water samples (350 µL) were mixed with equal volumes of 2-N HCl and loaded onto a 0.6 cm × 20 cm column of AG50WX8 cation-exchange resin, strontium was eluted with 2-N HCl, each Sr sample (150 ng) was then loaded onto a tungsten filament with a Ta_2O_5 substrate, and strontium samples were analyzed in dynamic multicollector mode on a VG sector thermal-ionization mass spectrometer. During the course of analyzing the ODP Leg 180 Sr isotope samples, National Bureau of Standards Standard Reference Material (SRM) 987 was analyzed 11 times, with an average $^{87}Sr/^{86}Sr = 0.710253$ and a total range of ±0.000022.

A subset of squeeze cakes from Site 1109 was selected for chemical and mineralogical analyses on the basis of the presence of volcanic matter in the sediments (Taylor, Huchon, Klaus, et al., 1999). The clay fraction was separated from the selected squeeze cakes by a combination of wet sieving and gravimetric methods as follows: samples were weighed after freeze drying and divided into a fine (<63 µm) and a coarse (>63 µm) fraction by wet sieving. Subsequent grain-size separation into a silt (2–63 µm) and a clay (<2 µm) fraction was performed by settling of par-

ticles in standing cylinders according to Stokes' law (Moore and Reynolds, 1989).

The clay mineralogy was determined by X-ray diffractometry (XRD), using a Philips model PW 1710 X-ray diffractometer equipped with monochromatic CuK_{α} radiation. Oriented samples were produced by vacuum filtration through a 0.15-µm filter. Measurements were carried out on air-dried and glycol-saturated samples. Randomly oriented powder preparations were produced (measurement made over 60–75°2θ) to identify di- or trioctahedral clay minerals from hkl = 060 reflections.

The clays were dissolved using a CEM model MDS100 microwave digestion system. Approximately 100 mg of each sample was placed in a Teflon reaction vessel, to which were added 500 µL of 18 ΩW-cm distilled deionized water, 6 mL of concentrated HF, and 4 mL of a 3:1 mixture of concentrated HNO_3:HCl. Samples were sealed, placed in the microwave oven, and digested until no visible residue remained. The vessels were allowed to cool, vented, and the solution evaporated to near dryness. The final paste was redissolved in 0.3-M HNO_3, diluted to ~100 g, and weighed to the nearest milligram. Quality control samples included approximately one blank and one SRM (NRC-Canada marine estuarine sediment: MESS-1) for every 10 samples and were carried through all procedures. Trace element concentrations in the digested clay samples were determined by ICP-MS after calibration with a series of multielement standards prepared from serial dilution of a NIST-traceable stock standard. Accuracy of our analyses was verified by comparison of our results for digestions of MESS-1 with other published values (e.g., Garbe-Schönberg, 1993).

RESULTS

Interstitial Water

Concentrations of dissolved Rb and Ba in IW from Sites 1109, 1115, and 1118 are presented in Table **T1;** isotopic compositions ($\delta^{18}O$ and $^{87}Sr/^{86}Sr$) are given in Table **T2.**

Substantial fluctuations in the concentrations of dissolved Ba (Fig. **F1**) occur downhole. Full depletion of SO_4^{2-} occurs between 100 and 200 mbsf at each site, although SO_4^{2-} reappears in IW deep within Site 1118 (Taylor, Huchon, Klaus, et al., 1999). The absence of SO_4^{2-} throughout a large part of the sedimentary column of each site allows dissolved Ba^{2+} to accumulate in the IW; yet, the shapes of the depth profiles as well as the range of Ba^{2+} concentrations vary between sites. Dissolved Ba^{2+} increases from <1 µM in the upper 50 mbsf (Site 1109) to 100 mbsf (Site 1115), to a maximum of 17.7 µM at 480 mbsf at Site 1109. Lesser fluctuations are observed at Sites 1115 and 1118, the latter displaying only about half the Ba^{2+} concentration range observed at Site 1109.

Dissolved Rb^{+} concentrations also vary widely throughout the sedimentary column of each site (Fig. **F1**). Concentrations reach two- to threefold enrichment over seawater in localized maxima within Pliocene sediments of Sites 1109 and 1115, although concentrations decrease sharply near the Miocene unconformity. Unlike what was observed for Ba^{2+}, the highest dissolved concentrations of Rb^{+} are present in IW from Site 1118, whereas variations in this constituent are most subdued at Site 1115, where Rb^{+} remains in a narrow range of ~2–2.5

T1. Trace element composition of interstitial water, p. 14.

T2. Isotopic composition of interstitial water, p. 17.

F1. Depth profiles of dissolved trace constituents, p. 8.

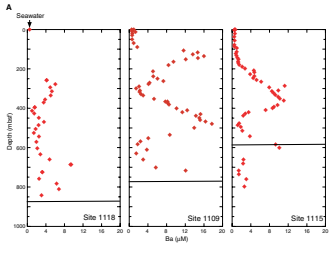

µM in the upper 400 mbsf. Dissolved Rb^+ is strongly depleted relative to seawater at and below the Miocene unconformity of Sites 1115 and 1109. A near total removal of Rb^+ from IW occurs near the bottom of Site 1109, whereas concentrations of Rb^+ remain more than twice that of bottom seawater in the deepest (842 mbsf) IW sample collected from Site 1118.

Sr isotope ratios display large variations in IW from the Woodlark Rise sites (Fig. F2). A systematic and similar decrease in $^{87}Sr/^{86}Sr$ with increasing depth is observed in the upper 300 mbsf of all three sites. Below this depth, however, values diverge. The widest range in $^{87}Sr/^{86}Sr$ ratio in the IW is observed at Site 1115, where it decreases from near-seawater values (e.g., $^{87}Sr/^{86}Sr$ = 0.70916) just below the mudline to a minimum of 0.70714 at 601 mbsf. The $^{87}Sr/^{86}Sr$ ratio increases slightly below 600 mbsf at Site 1115, before settling down near 0.708 in the deepest sections of the hole. IW from Site 1109 displays the narrowest range of $^{87}Sr/^{86}Sr$ values of the three Woodlark Rise sites, as well as a profile that mirrors that of Site 1115 between ~550 and 750 mbsf. In the deepest portion of Site 1109 the $^{87}Sr/^{86}Sr$ ratio decreases sharply again, approaching a value comparable to that observed at the same depth deep in Site 1118.

Profiles of oxygen isotopes in IW from the Woodlark Rise (Fig. F3) exhibit a general decrease in $\delta^{18}O$ downhole at Sites 1109 and 1115 and in the upper half of Site 1118 (i.e., 258–544 mbsf). At Sites 1109 and 1115 a small increase in the $\delta^{18}O$ is also observed between 20 and 50 mbsf. Unfortunately, because the upper 200 mbsf of the Site 1118 was drilled but not cored, no data are available for this depth range. At Site 1115, the largest decrease in $\delta^{18}O$ occurs across the Miocene unconformity, below which a minimum of –2.84‰ is observed at 667 mbsf. The trend in $\delta^{18}O$ values at Site 1109 is similar, although a much more subdued range is observed. The lowest value of –1.27‰ is present in the deepest sample (746 mbsf), which was recovered just above the Miocene unconformity. At Site 1118, there is a relatively steep negative gradient in $\delta^{18}O$ down to 544 mbsf where a value of –1.63‰ is recorded. However, unlike observed at the two other Woodlark Rise sites, a reversal in the $\delta^{18}O$ profiles occurs below 571 mbsf at Site 1118 and values trend back toward the contemporaneous seawater value, reaching –0.86‰ at 758 mbsf. Below 758 mbsf and approaching the Miocene unconformity, the profile resumes the decreasing trend in $\delta^{18}O$, as observed deep in the other Woodlark Rise sites. Overall, the range of $\delta^{18}O$ values at Site 1109 is small with the lowest value of –1.27‰ measured in the deepest sample (746 mbsf), which was recovered just above the Miocene unconformity.

Mineralogy and Trace Element Composition of Clays

The trace element composition of the clay fraction (<2 µm) of selected whole-round cores corresponding to the IW samples is shown in Table T3. The corresponding X-ray mineralogy is given in Table T4.

The trace element concentrations of the clay samples were normalized to the primitive mantle composition (Hofman, 1988) to help determined their provenance and elucidate the relationship of clays to the abundant volcanic matter dispersed throughout the sediments of Site 1109. The normalized data plotted as "spider diagrams" are shown in Figure F4. The clays generally exhibit similar patterns, with depletion of Nb and enrichment of Pb, Ti, and Hf noted for all samples. The slope of

F2. Depth profiles of the dissolved $^{87}Sr/^{86}Sr$ in interstitial water, p. 10.

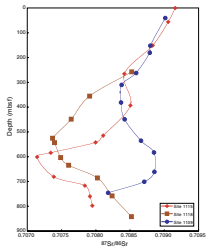

F3. Depth profiles of $\delta^{18}O$ of interstitial water, p. 11.

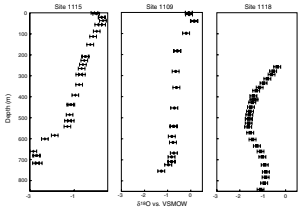

T3. Trace element composition of clays, p. 19.

T4. Mineralogical assemblages of clay fraction, p. 19.

F4. Spider diagrams of trace elements in clay, p. 12.

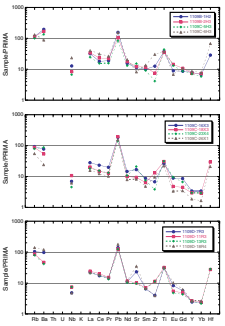

the patterns is steepest in the samples collected deep within Site 1109, except from Section 180-1109D-38R-4, whereas samples recovered from younger sediments display less fractionated patterns. The level of enrichment or depletion relative to the trend described by the other trace elements, however, is subject to substantial variability. Additionally, selected clays display enrichments in Sr and Zr (and to a lesser extent Gd). Some samples recovered deeper within the sedimentary column, especially between Section 180-1109C-39X-2 and Section 39R-2 show a greater Sr enrichment relative to other samples. In the case of Zr, however, the enrichment is more variable, with no uniform pattern observed with increasing depth downhole. In fact, some samples recovered from younger sediments display the highest Zr enrichment (e.g., Section 180-1109D-6H-3). Clay isolated from the conglomerate interval (Section 180-1109D-34R-4) exhibits the lowest trace element enrichment as well as less fractionation across the trace element series than clays isolated from younger sediments. The clay sample recovered from below the Miocene unconformity (e.g., Section 180-1109D-38R-4) exhibits little fractionation across the series of elements comprising the spider diagram, including lower normalized Rb and Ba abundances than most other clays, although it does not have the lowest overall trace element concentrations. The latter is particularly true toward the end of the trace element series (e.g., Ti, Eu, Gd, Y, and Yb), where this sample actually exhibits the highest enrichment of these elements.

XRD investigations were conducted to identify the mineral assemblages of the clay fraction and to determine the composition and distribution of the various minerals. Quartz, feldspar, and illite are considered of detrital origin in all holes, representing the background hemipelagic sedimentary supply (Taylor, Huchon, Klaus, et al. 1999). The presence of talc and serpentine minerals in Sections 180-1109C-10H-4 to 26X-1 indicates erosion of metamorphic rocks for which the D'Entrecasteaux Islands or Papuan Peninsula are the obvious source areas. The XRD data indicate the presence of a significant amount of mixed-layer chlorite/smectite clays, suggesting a distinctive provenance for these intervals. The increased abundance of smectite with increasing depth downhole is probably related to an increase of volcanic alteration supported by advanced devitrification of volcanic glass shards.

ACKNOWLEDGMENTS

This research used samples and/or data provided by the Ocean Drilling Program (ODP). ODP is sponsored by the U.S. National Science Foundation (NSF) and participating countries under management of Joint Oceanographic Institutions (JOI), Inc. Funding for this research was provided by a postcruise research grant to EDC from JOI/USSP. This is SOEST contribution No. 5572.

We wish to acknowledge the Captain and crew of the *JOIDES Resolution* and the ODP technical staff for a very successful cruise. We are particularly indebted to shipboard chemistry technicians Chieh Peng and Dennis Graham for their able assistance. C.M. Fraley and P. Carlton provided technical assistance at SOEST. P. Anschutz provided a review of this report.

REFERENCES

De Carlo, E.H., 1992. Geochemistry of pore water and sediments recovered from the Exmouth Plateau. *In* von Rad, U., Haq, B.U., et al., *Proc. ODP, Sci. Results,* 122: College Station, TX (Ocean Drilling Program), 295–308.

De Carlo, E.H., and Kramer, P.A., 2000. Minor and trace elements in interstitial waters of the Great Bahama Bank: results from ODP Leg 166. *In* Swart, P.K., Eberli, G.P., Malone, M.J., and Sarg, J.F. (Eds.), *Proc. ODP, Sci. Results,* 166: College Station TX (Ocean Drilling Program), 99–111.

Epstein, S., and Mayeda, T., 1953. Variation of ^{18}O content of waters from natural sources. *Geochim. Cosmochim. Acta,* 4:213–224.

Garbe-Schönberg, C.D., 1993. Simultaneous determination of 37 trace elements in 28 international rock standards by ICP/MS. *Geostand. Newsl.,* 17:81–97.

Hofman, A.W., 1988. Chemical differentiation of the Earth: the relationship between mantle, continental crust and oceanic crust. *Earth Planet. Sci. Lett.,* 90:297–314.

Mahoney, J., Nicollet, C., and Dupuy, C., 1991. Madagascar basalts: tracking oceanic and continental sources. *Earth Planet. Sci. Lett.,* 104:350–363.

Manheim, F.T., and Sayles, F.L., 1974. Composition and origin of interstitial waters of marine sediments, based on deep sea drill cores. *In* Goldberg, E.D. (Ed.), *The Sea* (Vol. 5): *Marine Chemistry: The Sedimentary Cycle:* New York (Wiley), 527–568.

Moore, D.M., and Reynolds, R.C., Jr., 1989. *X-ray Diffraction and the Identification and Analysis of Clay Minerals:* Oxford (Oxford Univ. Press).

Taylor, B., Huchon, P., Klaus, A., et al., 1999. *Proc. ODP, Init. Repts.,* 180 [CD-ROM]. Available from: Ocean Drilling Program, Texas A&M University, College Station, TX 77845-9547, U.S.A.

Tüchsen, E., Hayes, J.M., Ramaprasad, S., Copie, V., and Woodward, C., 1987. Solvent exchange of buried water and hydrogen exchange of peptide NH groups hydrogen bonded to buried water in bovine pancreatic trypsin inhibitor. *Biochemistry,* 26:5163–5172.

Figure F1. Depth profiles of dissolved trace constituents (**A**) Ba and (**B**) Rb in interstitial water from Sites 1109, 1115 and 1118 on the Woodlark Rise. The concentration of each constituent in seawater is indicated by an arrow at the top of the Site 1118 depth profile. The sedimentary unconformity at each site is shown by a solid line drawn across each profile at the appropriate depth. (**Continued on next page.**)

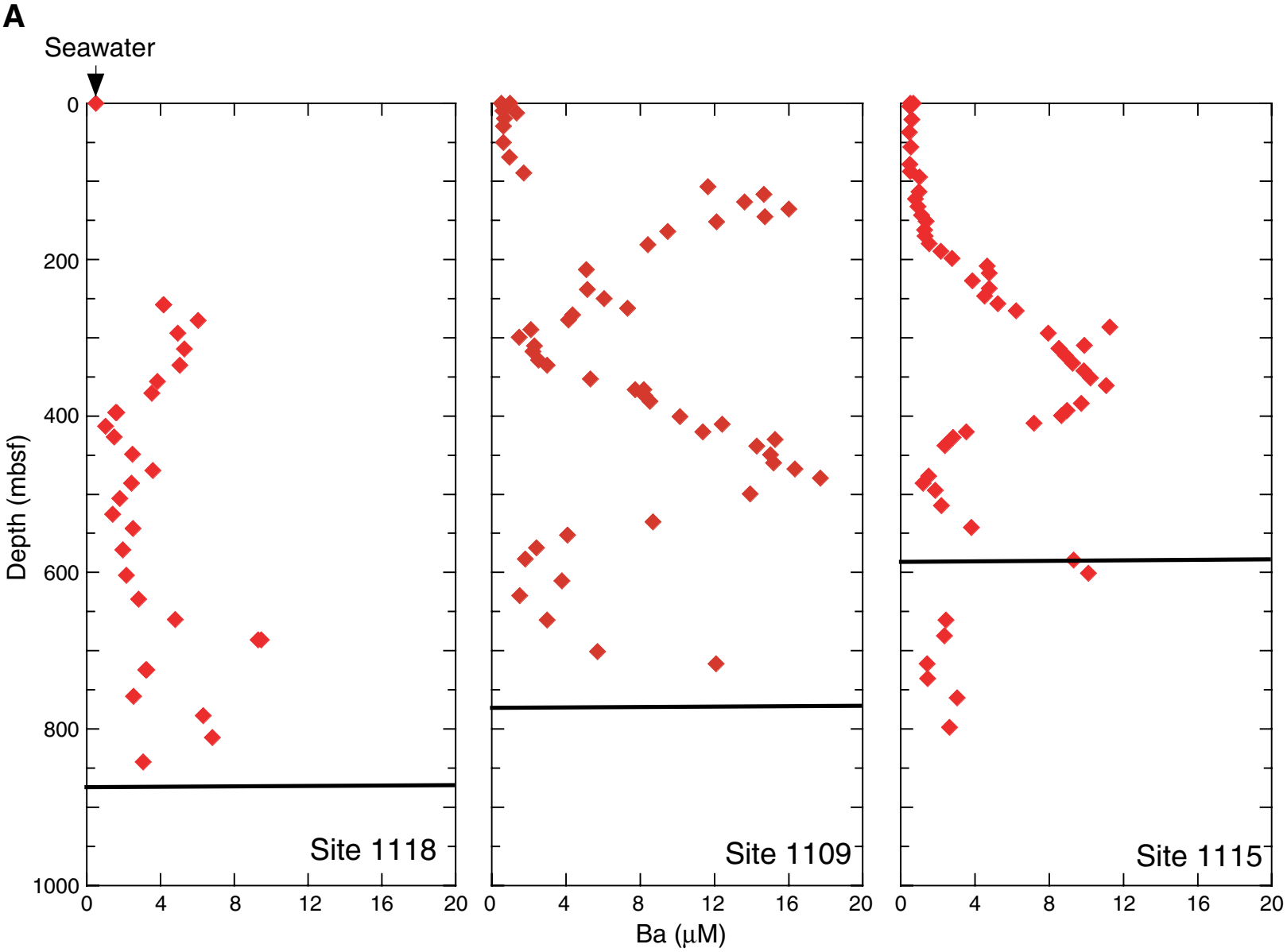

Figure F1 (continued). (Caption shown on previous page.)

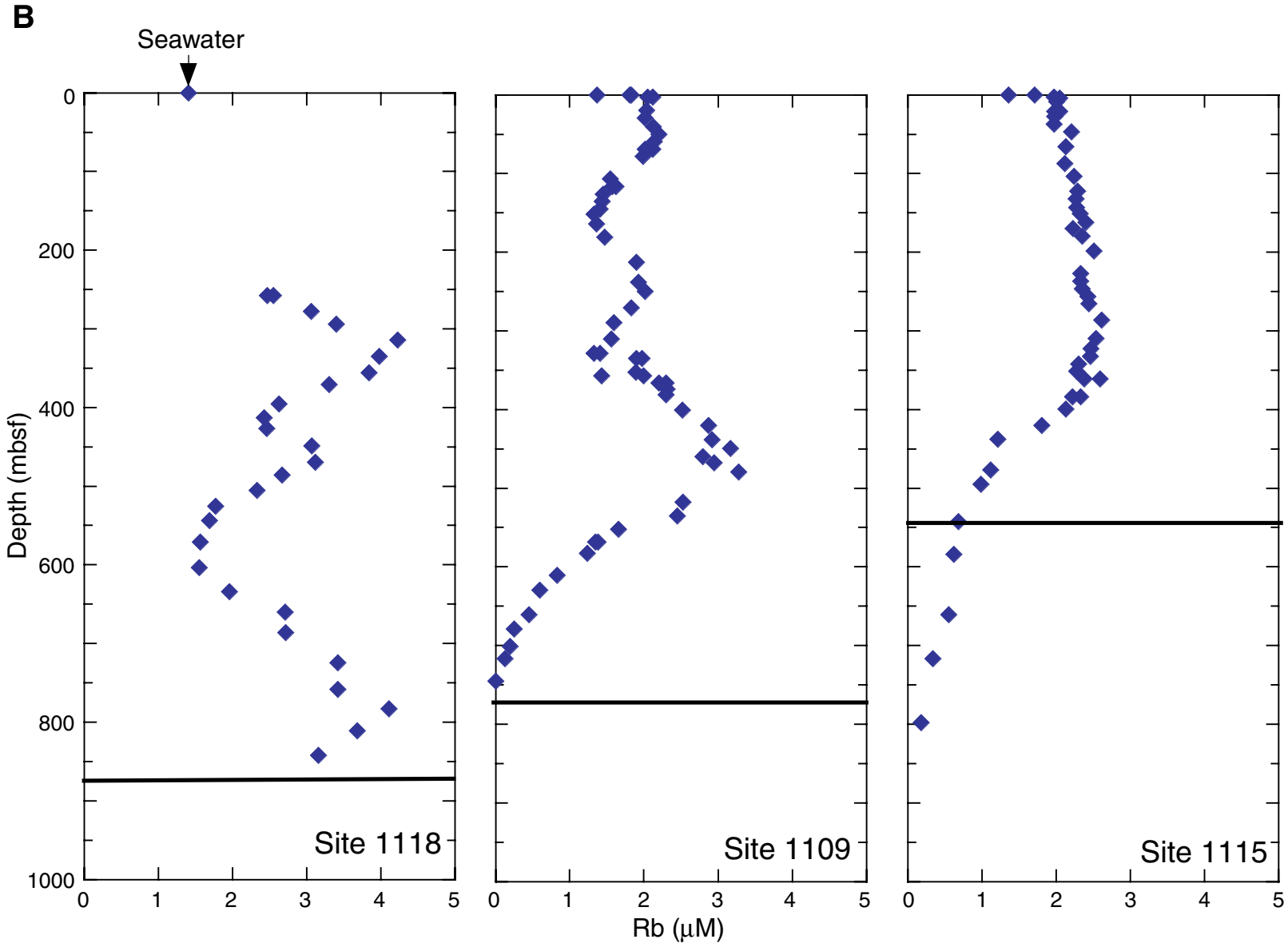

Figure F2. Depth profiles of the dissolved $^{87}Sr/^{86}Sr$ in interstitial water from Sites 1109, 1115, and 1118 on the Woodlark Rise. Solid circles = Site 1109, solid diamonds = Site 1115, solid squares = Site 1118.

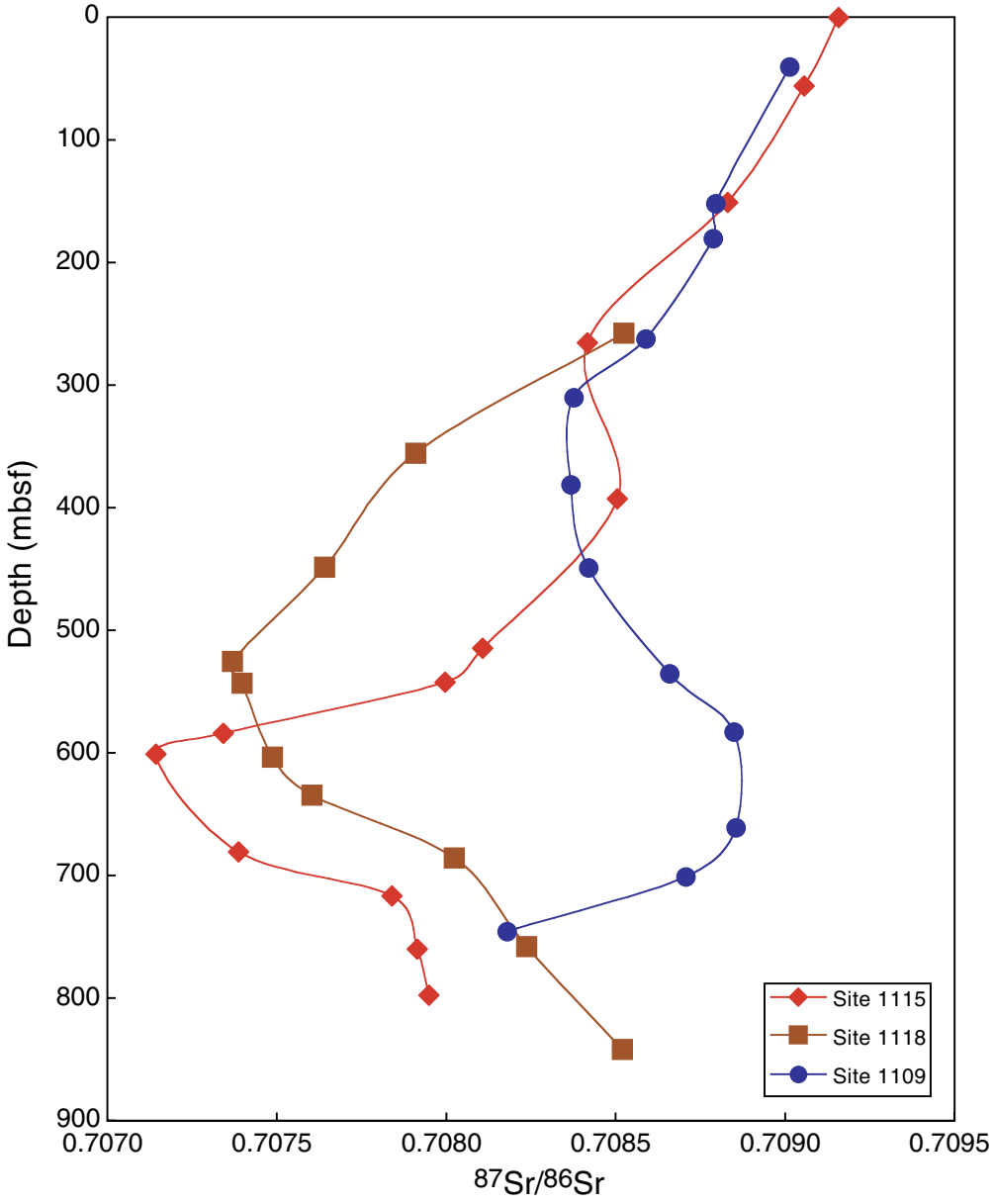

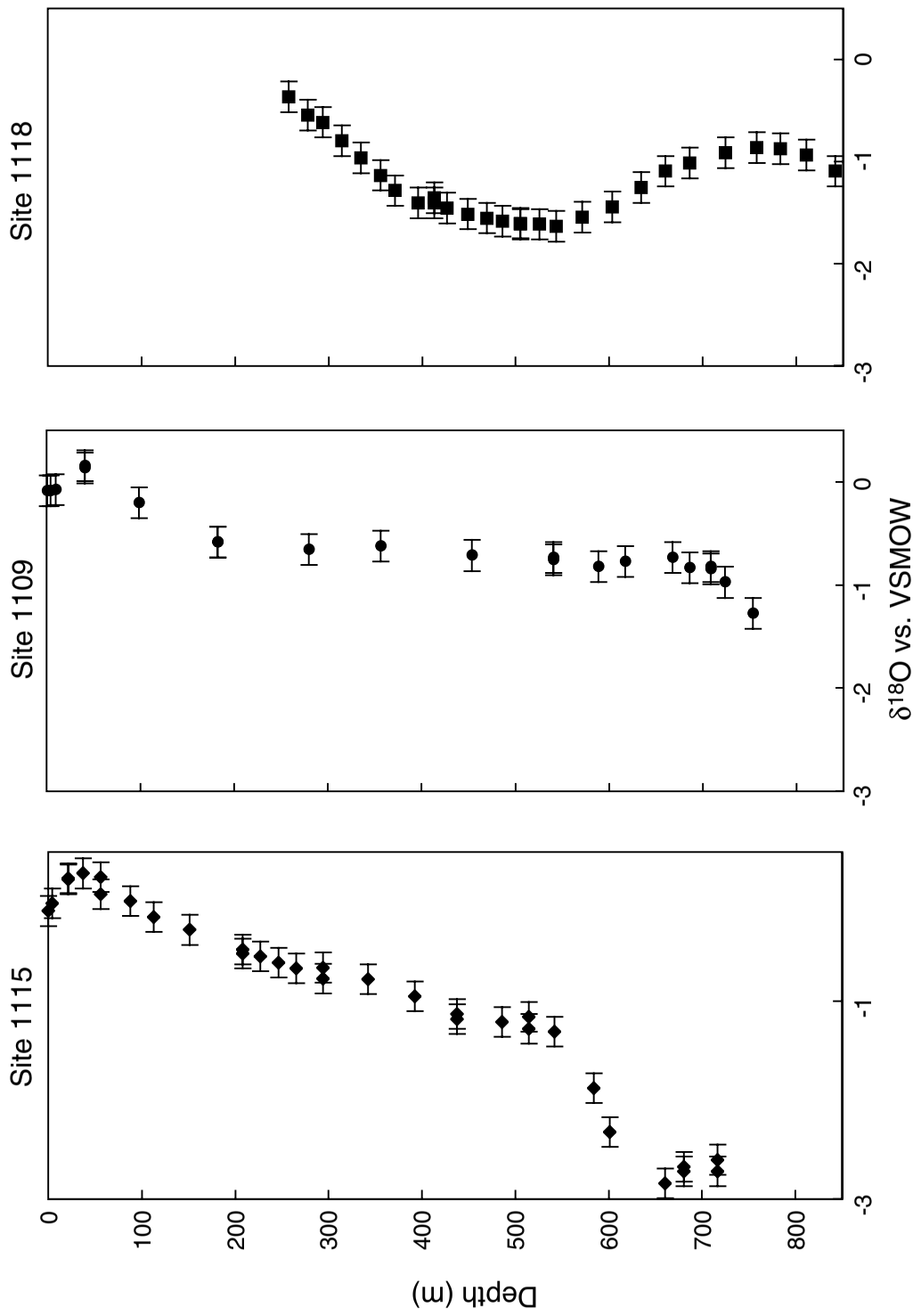

Figure F3. Depth profiles of $\delta^{18}O$ of interstitial water from Sites 1115, 1109, and 1118 on the Woodlark Rise. Error bars represent the instrumental precision for each measurement. VSMOW = Vienna standard mean ocean water.

Figure F4. Spider diagrams of trace elements in clays from Site 1109. All concentrations have been normalized to the primitive mantle (PRIMA) (Hoffman, 1988). (**Continued on next page.**)

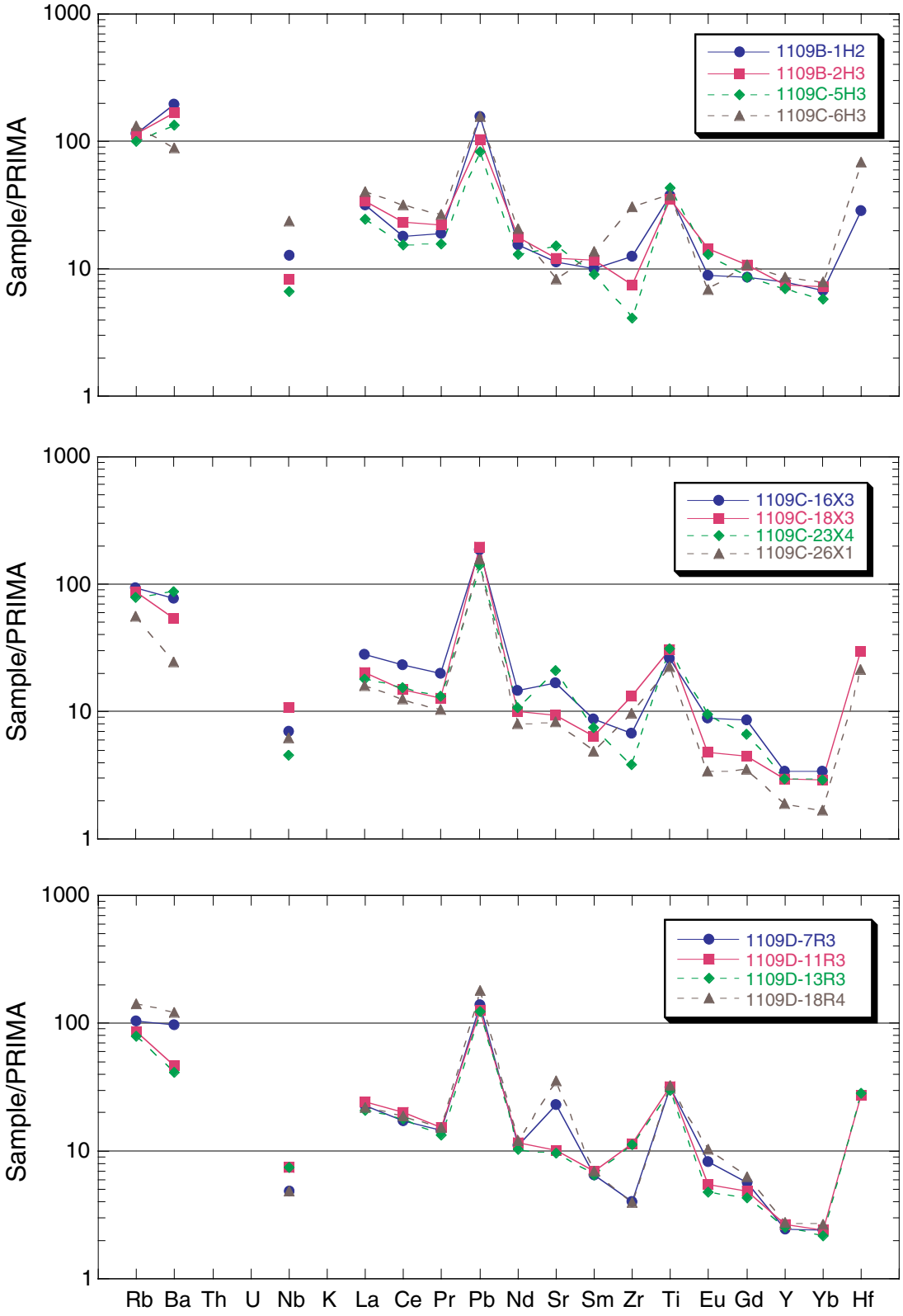

Figure F4 (continued). (Caption shown on previous page.)

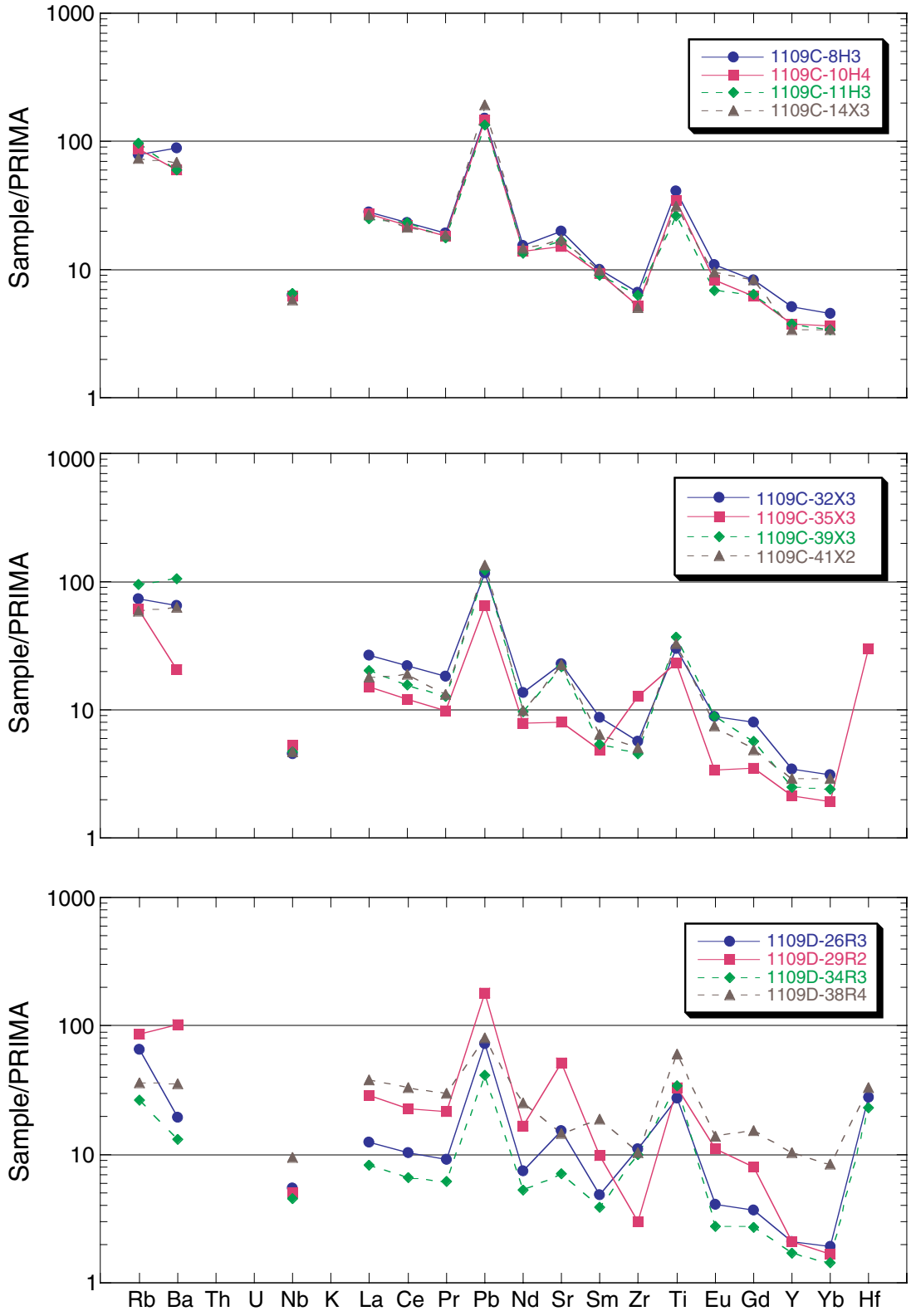

Table T1. Trace element composition of interstitial water, Sites 1109, 1115, and 1118. (See table note. Continued on next two pages.)

Core, section, interval (cm)	Depth (mbsf)	Ba (μM)		Ba (μM)	
		AES	ICP-MS	ICP-OES	ICP-MS
180-1109B-					
1H-1, 35–40	0.4	1.82		1.0	
1H-2, 145–150	2.9	2.09			
1H-3, 145–150	4.4			0.7	
2H-1, 145–150	6.8				
2H-3, 145–150	9.8			0.6	
2H-4, 75–80	10.6				
2H-5, 145–150	12.1			1.3	
2H-6, 145–150	13.6				
180-1109C-					
3H-2, 145–150	19.9	2.04		0.7	
4H-2, 145–150	29.4	2.02		0.6	
5H-3, 145–150	40.4	2.13			
6H-3, 145–150	49.9	2.20		0.6	
7H-3, 145–150	59.4	2.14			
8H-3, 145–150	68.9	2.12		0.9	
8H-3, 145–120	68.9	2.02			
9H-3, 145–150	78.4	1.99			
10H-4, 115–120	89.1			1.7	
12X-3, 145–150	106.9	1.55		11.7	
13X-3, 145–150	116.5	1.60		14.7	
14X-3, 145–150	126.1	1.44		13.6	
15X-3, 145–150	135.6	1.44		16.0	
16X-3, 145–150	145.3	1.41		14.7	
17X-1, 145–150	152	1.33		12.1	
18X-3, 115–120	164.3	1.36		9.5	
20X-1, 140–150	180.7	1.47		8.4	
23X-4, 33–43	212.4	1.90		5.1	
26X-1, 140–145	238.4	1.93		5.2	
27X-2, 140–150	249.6	2.02		6.1	
28X-4, 140–150	262.2			7.3	
29X-3, 140–150	270.4	1.83		4.4	
30X-1, 140–150	277			4.1	
31X-3, 140–150	289.5	1.60		2.1	
32X-3, 140–150	299.2			1.5	
33X-4, 115–120	310.2	1.56		2.3	
34X-2, 140–150	317.1			2.2	
35X-3, 140–150	328.3	1.37		2.5	
36X-1, 140–150	334.9	1.94		3.0	
38X-4, 140–150	352.5	1.89		5.3	
39X-3, 140–150	357	1.43			
40X-3, 110–120	366.3	2.20		7.7	
41X-2, 140–150	374.4	2.31		8.3	
180-1109D-					
2R-6, 96–106	365.9	2.30		8.2	
4R-3, 96–106	381.6	2.30		8.5	
6R-3, 97–107	401	2.52		10.1	
7R-3, 120–130	410.7			12.4	
8R-3, 141–151	420.3	2.87		11.4	
9R-3, 101–111	430.1			15.3	
10R-2, 131–141	438.4	2.92		14.3	
11R-3, 122–132	449.3	3.17		15.0	
12R-4, 120–130	460.1	2.80		15.2	
13R-3, 79–89	467.9	2.95		16.3	
14R-4, 136–146	479.3	3.28		17.7	
16R-5,	499.7			13.9	
18R-4, 120–130	517.7	2.53			
20R-3, 65–75	535.4	2.45		8.7	
22R-1, 124–134	552.4	1.66		4.1	
24R-2, 135–148	568.4	1.38		2.4	
24R-2, 135–148	568.4	1.35			
26R-3, 30–40	583	1.24		1.8	
29R-2, 93–103	610.9	0.83		3.8	
31R-1, 130–140	629.5	0.60		1.5	
34R-3, 123–133	661	0.45		3.0	

Table T1 (continued).

Core, section, interval (cm)	Depth (mbsf)	Ba (μM)		Ba (μM)	
		AES	ICP-MS	ICP-OES	ICP-MS
36R-2, 140–150	679.3	0.25			
38R-4, 140–150	701.2	0.20		5.7	
40R-2, 29–39	716.6	0.13		12.1	
43R-2, 82–89	745.7	0.00			
180-1115A-					
1H-1, 23–28	0.23	1.71		0.7	
1H-3, 145–150	2.95	1.97			
1H-4, 115–120	4.15	2.05		0.5	
180-1115B-					
2H-1, 145–150	8.65	2.01			
3H-3, 145–150	21.15	2.02		0.6	
4H-1, 145–150	27.65	1.98			
5H-1, 145–150	37.15	1.97		0.5	
6H-1, 145–150	46.65	2.21			
7H-1, 145–150	56.15			0.6	
8H-1, 145–150	65.65	2.13			
9H-3, 145–150	78.15			0.5	
10H-3, 145–150	87.65	2.12		0.5	
11H-1, 145–150	94.15			1.0	
12H-1, 145–150	103.65	2.24			
13H-1, 145–150	113.15			1.0	
14H-1, 145–150	122.65	2.29		0.8	
15H-1, 145–150	132.15	2.27		0.9	
16H-2, 145–150	143.15	2.28		1.1	
17H-1, 145–150	151.15	2.32		1.4	
18H-2, 145–150	162.15	2.40		1.3	
19H-1, 145–150	170.15	2.23		1.3	
20H-1, 145–150	179.65	2.35		1.5	
21H-1, 145–150	189.15			2.2	
22H-1, 145–150	198.65	2.51		2.8	
23H-1, 145–150	208.15			4.7	
24X-1, 145–150	217.65			4.8	
25X-1, 145–150	227.25	2.33		3.9	
26X-1, 115–120	236.55	2.33		4.8	
27X-1, 145–150	246.45	2.35		4.5	
28X-1, 145–150	256.05	2.43		5.2	
29X-1, 145–150	265.75	2.44		6.2	
31X-2, 145–150	286.45	2.61		11.3	
180-1115C-					
2R-1, 144–150	294.24			7.9	
3R-5, 115–120	309.65	2.54		9.9	
4R-1, 146–151	313.56			8.5	
5R-1, 120–127	322.9	2.47		8.9	
6R-1, 140–145	332.8	2.46		9.3	
7R-1, 141–146	342.41	2.30		9.9	
8R-1, 79–84	351.39	2.28		10.2	
9R-1, 113–119	361.03	2.49		11.1	
10R-1, 145–150	370.95				
11R-4, 30–41	383.72	2.28		9.7	
12R-3, 130–140	392.8			9.0	
13R-2, 0–14	399.6	2.13		8.7	
14R-1, 135–144	409.05			7.2	
15R-2, 140–150	420.2	1.81		3.5	
16R-1 69–79	427.59			2.8	
17R-1, 109–119	437.59	1.21		2.4	
21R-2, 86–96	476.58	1.12		1.5	
22R-1 140–150	485.9			1.2	
23R-1, 123–138	495.33	0.99		1.9	
25R-1, 140–150	514.8			2.2	
28R-1, 20–30	542.4	0.68		3.8	
32R-3, 116–126	584.11	0.62		9.3	
34R-1, 138–148	601.18			10.1	
40R-2, 140–150	660.7	0.55		2.5	
42R-3, 140–150	680.79			2.4	
44R-1, 98–108	697.48				
46R-1, 105–115	716.75	0.34		1.4	
48R-1, 78–88	735.88			1.5	

Table T1 (continued).

Core, section, interval (cm)	Depth (mbsf)	Ba (μM)		Ba (μM)	
		AES	ICP-MS	ICP-OES	ICP-MS
50R-5, 90–102	760.13			3.0	
52R-1, 103–113	774.63				
54R-4, 140–150	798.14	0.18		2.6	
180-1118A-					
6R-4, 140–150	257.8	2.51	2.12		4.19
8R-4, 140–150	278	3.06	2.72		6.07
10R-2, 140–150	294.3	3.40	3.03		4.95
12R-3, 111–121	314.3	4.23	3.63		5.34
14R-4, 131–141	335.1	3.98	3.60		5.01
16R-5, 91–101	355.9	3.84	3.42		3.83
18R-2, 128–137	371	3.30	3.02		3.58
20R-6, 134–146	395.8	2.63	2.41		1.63
20R-6, 134–146	395.8	2.40	2.40		1.57
22R-5, 112–123	413.1	2.43	2.23		1.05
24R-1, 134–146	426.9	2.46	2.22		1.53
26R-3, 110–119	448.9	3.07	2.78		2.48
28R-4, 107–117	469.4	3.12	2.89		3.58
30R-2, 132–142	486	2.67	2.44		2.44
32R-2, 131–141	505.3	2.33	2.08		1.81
34R-3, 116–131	525.7	1.77	1.63		1.41
36R-2, 135–145	543.5	1.69	1.56		2.46
39R-1, 138–150	571.4	1.57	1.44		2.00
42R-4, 98–110	603.6	1.55	1.40		2.15
45R-6, 92–102	634.6	1.96	1.76		2.82
48R-3, 112–122	660.4	2.71	2.44		4.77
51R-1, 74–89	686		2.79		9.22
51R-1, 74–89	686	2.72	2.85		9.42
55R-1, 72–87	724.8	3.42	3.42		3.17
55R-1, 72–87	724.8		3.57		3.25
58R-4, 135–150	758.2	3.42	3.57		2.49
61R-1, 113–128	783	4.11	4.04		6.24
64R-1, 9–21	810.8	3.68	3.98		6.81
67R-2, 135–150	842.2	3.13	2.52		3.12

Note: AES = atomic emission spectroscopy, ICP-MS = inductively coupled plasma–mass spectroscopy, ICP-OES = inductively coupled plasma–optical emission spectroscopy.

Table T2. Isotopic composition of interstitial water, Sites 1109, 1115, and 1118. (Continued on next page.)

Core, section, interval (cm)	Depth (mbsf)	$^{87}Sr/^{86}Sr$	2-σ uncertainty	Replicate $^{87}Sr/^{86}Sr$	2-σ uncertainty	$\delta^{18}O$	Replicate $\delta^{18}O$
180-1109B-							
1H-1, 35–40	0.4					–0.08	
1H-3, 145–150	4.4					–0.08	
2H-3, 145–150	9.8					–0.07	
180-1109C-							
5H-3, 145–150	40.4	0.709014	0.000016			0.16	0.14
11H-3, 145–150	97.4					–0.2	
17X-1, 145–150	152.0	0.708796	0.000013				
20X-1, 140–150	180.7	0.708788	0.000016			–0.58	
28X-4, 140–150	262.2	0.708590	0.000013				
30X-1, 140–150	277.0					–0.65	
33X-4, 115–120	310.2	0.708377	0.000014				
38X-4, 140–150	352.5					–0.62	
180-1109D-							
4R-3, 96–106	381.6	0.708368	0.000013				
11R-3, 122–132	449.3	0.708420	0.000014			–0.71	
20R-3, 65–75	535.4	0.708660	0.000013			–0.75	
26R-3, 30–40	583.0	0.708850	0.000016			–0.82	
29R-2, 93–103	610.9					–0.77	
34R-3, 123–133	661.0	0.708856	0.000014			–0.73	
36R-2, 140–150	679.3					–0.83	
38R-4, 140–150	701.2	0.708708	0.000014			–0.84	
40R-2, 29–39	716.6					–0.97	
43R-2, 82–89	745.7	0.708179	0.000014			–1.27	
180-115A-							
1H-1, 23–28	0.2	0.709159	0.000014			–0.09	
1H-4, 115–120	4.2					–0.01	
180-1115B-							
3H-3, 145–150	21.2					0.23	0.24
5H-1, 145–150	37.2					0.29	
7H-1, 145–150	56.2	0.709057	0.000017			0.08	0.25
10H-3, 145–150	87.7					0.01	
13H-1, 145–150	113.2					–0.15	
17H-1, 145–150	151.2	0.708832	0.000014			–0.28	
23H-1, 145–150	208.2					–0.52	–0.48
25X-1, 145–150	227.3					–0.55	
27X-1, 145–150	246.5					–0.61	
29X-1, 145–150	265.8	0.708418	0.000014	0.708443	0.000014	–0.67	
180-1115C-							
2R-1, 144–150	294.2					–0.77	–0.66
7R-1, 141–146	342.4					–0.78	
12R-3, 130–140	392.8	0.708506	0.000013			–0.95	
17R-1, 109–119	437.6					–1.18	–1.13
22R-1, 140–150	485.9					–1.21	
25R-1, 140–150	514.8	0.708108	0.000016			–1.28	–1.16
28R-1, 20–30	542.4	0.707998	0.000016			–1.31	
32R-3, 116–126	584.1	0.707343	0.000014			–1.88	
34R-1, 138–148	601.2	0.707143	0.000013			–2.32	
40R-2, 140–150	660.7					–2.84	
42R-3, 140–150	680.8	0.707388	0.000014			–2.72	–2.67
46R-1, 105–115	716.8	0.707841	0.000013			–2.6	–2.72
50R-5, 90–102	760.1	0.707915	0.000016				
54R-4, 140–150	798.1	0.707949	0.000014				
180-1118A-							
6R-4, 140–150	257.8	0.708525	0.000014			–0.36	–0.54
8R-4, 140–150	278.0					–0.54	
10R-2, 140–150	294.3					–0.61	
12R-3, 111–121	314.3					–0.79	
14R-4, 131–141	335.1					–0.96	
16R-5, 91–101	355.9	0.707910	0.000016			–1.13	
18R-2, 128–137	371.0					–1.28	
20R-6, 134–146	395.8					–1.4	
22R-5, 112–123	413.1					–1.35	–1.4
24R-1, 134–146	426.9					–1.45	
26R-3, 110–119	448.9	0.707642	0.000016			–1.51	

Table T2 (continued).

Core, section, interval (cm)	Depth (mbsf)	$^{87}Sr/^{86}Sr$	2-σ uncertainty	Replicate $^{87}Sr/^{86}Sr$	2-σ uncertainty	$\delta^{18}O$	Replicate $\delta^{18}O$
28R-4, 107–117	469.4					–1.55	
30R-2, 132–142	486.0					–1.58	
32R-2, 131–141	505.3					–1.6	–1.61
34R-3, 116–131	525.7	0.707370	0.000017	0.707385	0.000017	–1.61	
36R-2, 135–145	543.5	0.707397	0.000014			–1.63	
39R-1, 138–150	571.4					–1.54	
42R-4, 98–110	603.6	0.707487	0.000014			–1.44	
45R-6, 92–102	634.6	0.707604	0.000014			–1.25	
48R-3, 112–122	660.4					–1.09	
51R-1, 74–89	686.0	0.708024	0.000014			–1.01	
55R-1, 72–87	724.8					–0.91	
58R-4, 135–150	758.2	0.708238	0.000013			–0.86	
61R-1, 113–128	783.0					–0.87	
64R-1, 9–21	810.8					–0.93	
67R-2, 135–150	842.2	0.708521	0.000016			–1.09	

Table T3. Trace element composition of clays isolated from interstitial water squeeze-cake samples, Site 1109.

Core, section, interval (cm)	Depth (mbsf)	Rb (µg/g)	Ba (µg/g)	Nb (µg/g)	La (µg/g)	Ce (µg/g)	Pr (µg/g)	Pb (µg/g)	Nd (µg/g)	Sr (µg/g)	Sm (µg/g)	Zr (µg/g)	Ti (µg/g)	Eu (µg/g)	Gd (µg/g)	Y (µg/g)	Yb (µg/g)	Hf (µg/g)
180-1109B-																		
1H-2, 145–150	2.9	62.0	1190	7.9	19.5	29.0	4.6	27.2	18.4	205	3.9	123	6779	1.3	4.4	31.1	2.8	7.7
2H-3, 145–150	9.8	61.5	1016	5.1	20.9	37.6	5.3	18.2	21.0	220	4.5	73	6394	2.1	5.5	29.4	3.0	
180-1109C-																		
5H-3, 145–150	40.4	53.4	808	4.1	15.0	24.5	3.8	14.6	15.5	275	3.5	40	7759	1.9	4.4	27.6	2.4	
6H-3, 145–150	49.9	70.1	534	14.6	24.7	51.0	6.4	27.4	24.4	150	5.3	296	6767	1.0	5.5	34.2	3.3	18.2
8H-3, 145–150	68.9	42.0	533	3.9	17.3	37.0	4.7	26.2	18.4	360	3.9	65	7407	1.6	4.3	20.4	1.9	
10H-4, 115–120	89.1	46.7	360	3.8	16.7	35.3	4.4	25.5	16.6	278	3.6	51	6278	1.2	3.2	14.9	1.5	
11H-3, 145–150	97.4	51.9	361	4.0	15.4	37.3	4.3	23.5	16.1	304	3.5	62	4743	1.0	3.3	14.9	1.4	
14X-3, 145–150	126.1	39.3	417	3.6	16.3	34.2	4.5	33.3	17.3	311	3.8	49	5587	1.4	4.3	13.5	1.4	
16X-3, 145–150	145.3	49.6	470	4.3	17.4	37.0	4.8	32.4	17.5	303	3.4	65	4749	1.3	4.4	13.4	1.4	
18X-3, 115–120	164.3	46.6	328	6.6	12.4	23.9	3.1	34.0	11.9	172	2.5	129	5558	0.7	2.3	11.8	1.2	7.9
23X-4, 33–43	212.4	42.3	526	2.8	11.1	24.6	3.2	24.6	12.8	380	2.9	38	5606	1.4	3.4	11.7	1.2	
23X-4, 33–43	212.4	41.4	532	2.9	13.1	28.1	3.6	22.9	13.8	382	2.9	40	6203	1.3	2.9	12.5	1.1	
26X-1, 140–145	238.4	29.8	149	3.8	9.7	20.2	2.5	27.2	9.6	151	1.9	94	4071	0.5	1.8	7.5	0.7	5.7
32X-3, 140–150	299.2	39.4	392	2.8	16.4	35.4	4.4	20.3	16.3	416	3.4	56	5457	1.3	4.1	13.7	1.3	
32X-3, 140–150	299.2	38.8	380	2.8	16.0	34.5	4.1	19.7	14.8	390	2.7	59	5689	1.1	3.1	12.2	1.1	
35X-3, 140–150	328.3	32.6	124	3.3	9.3	19.5	2.4	11.3	9.4	147	1.9	124	4200	0.5	1.8	8.5	0.8	8.0
39X-3, 140–150	357.0	50.4	635	2.9	12.4	25.2	3.1	21.4	11.5	394	2.1	44	6712	1.3	2.9	9.9	1.0	
41X-2, 140–150	374.4	31.3	384	2.9	11.0	30.3	3.2	23.3	11.8	409	2.5	49	5927	1.1	2.5	11.5	1.2	
180-1109D-																		
7R-3, 120–130	410.7	56.0	584	3.0	13.8	27.8	3.5	24.3	13.1	423	2.5	39	5664	1.2	2.9	9.6	1.0	
11R-3, 122–132	449.3	45.9	283	4.6	14.9	32.4	3.7	22.1	13.8	185	2.7	110	5827	0.8	2.5	10.5	1.0	7.3
13R-3, 79–89	467.9	42.4	249	4.6	12.8	28.3	3.2	21.6	12.3	175	2.5	109	5417	0.7	2.2	9.9	0.9	7.6
18R-4, 120–130	517.7	76.2	737	3.0	13.4	30.1	3.7	31.4	14.3	647	2.7	39	5883	1.5	3.2	10.9	1.1	
26R-3, 30–40	583.0	34.9	118	3.4	7.7	16.6	2.2	12.8	8.9	281	1.9	107	4961	0.6	1.9	8.3	0.8	7.5
29R-2, 93–103	610.9	46.0	620	3.1	17.7	36.2	5.2	31.6	20.0	940	3.8	29	5993	1.6	4.1	8.3	0.7	
29R-2, 93–103	610.9	54.7	692	3.1	20.4	44.3	5.7	32.4	21.5	976	4.2	35	6011	1.8	4.1	9.7	1.0	
34R-3, 123–133	661.0	14.1	80	2.8	5.1	10.7	1.5	7.3	6.3	130	1.5	96	6175	0.4	1.4	6.7	0.6	6.2
38R-4, 140–150	701.2	19.2	215	5.9	23.4	53.3	7.2	14.0	30.1	263	7.3	100	10961	2.0	7.9	40.7	3.5	8.8

Table T4. Mineralogical assemblages of the clay fraction of sediments, Holes 1109B, 1109C, and 1109D.

Core, section, interval (cm)	Depth (mbsf)	Quartz	Feldspar	Pyrite	Magnesite	Clinoptinolite	Illite	Talc	Serpentine	Smectite	C/S	Chlorite
180-1109B-												
1H-2, 145–150	2.9	xx	x				x			xx		xx
2H-3, 145–150	9.8	xx	x				x				xx	xx
2H-5, 145–150	12.1	xx	x	x			x			xx		xx
180-1109C-												
3H-2, 145–150	19.9	xx	x	*			x					xx
5H-3, 145–150	40.4	xx	x (P)				x			xx		xx
6H-3, 145–150	49.9	xx	x (P)				x				xx	xx
8H-3, 145–150	68.9	xx	x (P)				*			xx		xx
10H-4, 115–120	89.1	xx	x				*	xx	xx		xx	xx
11H-3, 145–150	97.0	xx	x		*		*	xx	xx		xx	xx
14X-3, 145–150	126.1	xx	x	*			*	xx	xx	xx		xx
16X-3, 145–150	145.3	xx	x				*	xx	xx	xx		xx
18X-3, 115–120	164.3	xx	x	*			*	xx	xx	xxx	xx	
23X-3, 33–43	212.4	xx	x				*	xx	xx	xx		xx
26X-1, 140–145	238.4	x	x		x			xx	xx	xx		xx
29X-3, 140–150	270.4	x	xx (P)	*			*			xx		xx
32X-3, 140–150	299.2	xx	x				*			xx		xxx
180-1109D-												
35X-3, 140–150	328.3	xx	x				*			xxx		x
180-1109C-												
39X-3, 140–150	357.0	x	x			xx	*			xxx		x
41X-2, 140–150	374.4	xx	x				*			xx		x
180-1109D-												
7R-3, 120–130	410.7	xx	x				*			xx		x
9R-3, 101–111	430.1	xx	xx				x				xx	xx
11R-3, 122–132	449.3	xx	xx				*				xx	xx
13R-3, 79–89	467.9	xx	x	*			*			xxx		x
16R-5, 120–130		xx	x	*			*					xxx
18R-4, 120–130	517.7	xx	x				x			xx		x
22R-1, 124–134	552.4	*	*			xx	*			xx		x
26R-3, 30–40	583.0	xx	x				*			xxx		x
29R-2, 93–103	610.9	xx	xx (P)	x			*			xx		xx
34R-3, 123–133	661.0	x	*				*			xxx		x ?
38R-4, 150–150	701.4	xx	x				*	x		xxx		x

Notes: Assemblages were determined by X-ray diffraction analyses. C/S = chlorite-smectite mixed-layer, (P) = including feldspar. xxx = abundant, xx = common, x = rare, * = trace.